Agrociencia

COMPUTATIONAL ANALYSIS OF THE EFFECT OF AN EXTERNAL BARRIER ON THE VENTILATION AND THERMAL PERFORMANCE OF A GREENHOUSE

Mirka Maily **Acevedo-Romero**[1], Cruz Ernesto **Aguilar-Rodríguez**[2], Constantin Alberto **Hernández-Bocanegra**[1*], José Ángel **Ramos-Banderas**[1], Gildardo **Solorio-Díaz**[3]

[1]Instituto Tecnológico de Morelia. Doctorado en Ingeniería. Avenida Tecnológico 1500, Morelia, Michoacán, Mexico. C. P. 58120.
[2]Instituto Tecnológico Superior de los Reyes. Carretera Jacona-Los Reyes, Libertad, Los Reyes de Salgado, Michoacán, Mexico. C. P. 60300.
[3]Universidad Michoacana de San Nicolás de Hidalgo. Posgrado en Ingeniería Mecánica. C. de Santiago Tapia 403, Centro, Morelia, Michoacán, Mexico. C. P. 58030.
* Author for correspondence: constantin.hb@morelia.tecnm.mx

Citation: Acevedo-Romero MM, Aguilar-Rodríguez CE, Hernández-Bocanegra CA, Ramos-Banderas JA, Solorio-Díaz G. 2025. Computational analysis of the effect of an external barrier on the ventilation and thermal performance of a greenhouse. **Agrociencia.** https://doi.org/ 10.47163/agrociencia.v59i4.3296

Editor in Chief:
Dr. Fernando C. Gómez Merino

Received: September 04, 2024.
Approved: May 12, 2025.
Published in Agrociencia: June 12, 2025.

ABSTRACT

The construction of greenhouses in semi-urban areas implies the presence of neighboring buildings that can be an obstacle to natural ventilation, modifying the intensity and direction of air currents. However, they could also function as protective barriers against these currents at off-peak hours. The objective of this work was to analyze the effect of an external physical barrier on the thermal behavior and air currents inside a Gothic type greenhouse for tomato (*Solanum lycopersicum* L.) production. A 3D steady-state simulation was performed and validated using 15-day experimental temperature data with typical climatic conditions for the month of July 2023. The effect of the 3 m high external barrier was analyzed, which was placed at 5, 10, and 15 m distance from the greenhouse, located in the direction of the prevailing winds, on the fluid dynamic and thermal behavior inside the greenhouse. The results showed differences in the behavior of air currents inside the greenhouse with the presence of the external barrier, which affected the velocity and direction of the air inlet, accentuated by the proximity between the obstacle and the greenhouse. Under the studied conditions, placing the barrier 5 m away represents an advantage when there are low temperatures at dawn, managing to preserve the temperature inside the greenhouse up to 4 °C above the temperatures recorded in the barrier-free scenario or with the barrier 10 and 15 m away. The simulated data at 14:00 h showed differences of less than 0.4 °C between the cases with different barrier distances, so the influence of the barrier at the above-mentioned time is not significant.

Keywords: computational fluid dynamics, turbulence, external physical barrier.

INTRODUCTION

The use of greenhouses for food production is currently a viable option to meet food demand in many countries. These structures allow partial control of variables such

as temperature, humidity, CO_2 concentration, and radiation, which allow optimal plant development (Flores-Velázquez and Ojeda-Bustamante, 2015) and improve the standard of living of the population with fresh food all year round (El-Alaoui *et al*., 2023). In Mexico, most greenhouses in the country operate through empirical knowledge (Aguilar-Rodríguez *et al*., 2020a). The use of computational fluid dynamics in protected agriculture stems from the need for a detailed understanding of the physicochemical processes that take place in these systems (Flores-Velázquez and Ojeda-Bustamante, 2015; Aguilar-Rodríguez *et al*., 2021; Bournet and Rojano, 2022). In passively ventilated greenhouses, air intake and its velocity are determinant in the management of the indoor climate; this type of ventilation is currently the most widely used in tropical and subtropical countries due to its low or no maintenance cost (Villagrán *et al*., 2019; Ortiz-Rocha *et al*., 2021).

The importance and influence of wind velocity and direction on temperature control have been reported inside the greenhouse through different combinations of window opening and closing (Espinoza *et al*., 2017; He *et al*., 2018; Li *et al*., 2020). On the other hand, studies on the behavior of wind currents and temperature in greenhouses with three (Espinoza *et al*., 2017) or more bays (Ruiz-García *et al*., 2015; Aguilar-Rodríguez *et al*., 2021) have been conducted to determine the thermal behavior under natural ventilation, highlighting the combination of window opening, wind direction, and comparisons between structures such as saw, hood, and arched types.

In greenhouses with ridge vents, ventilation rates are best when they are open and perpendicular to the wind direction (Chu and Lan, 2019). Wind direction and temperature are affected by the zenith window; however, this effect is negligible at the plant level, and humidity is lower below the windward window (Akrami *et al*., 2020). Similarly, ventilation in living spaces and how the proximity of these assemblies can affect air currents and temperature have been studied (Carpentieri and Robins, 2015; Castro *et al*., 2017; King *et al*., 2017).

Greenhouse construction is aimed at production intensification with the greatest possible cost reduction. To this end, different environmental factors are taken into consideration during their construction, such as the direction of prevailing winds, latitude and altitude of the site, geometry of the building, window configuration, and radiation (Flores-Velázquez and Ojeda-Bustamante, 2015; Villagrán *et al*., 2020a; Choab *et al*., 2019). Currently, the use of space for greenhouse construction is a factor to be considered due to the interaction of contiguous built-up areas. The growth of protected agriculture in recent years has taken place in semi-urbanized areas with the presence of buildings or natural barriers.

Simulations in the study by Ghoulem *et al*. (2020) showed that greenhouses with wind traps provided higher ventilation rates than side windows when nearby structures are present. Villagrán and Bojacá (2019), on the other hand, studied the effect of natural obstacles on the thermal performance of passively ventilated greenhouses, finding that the presence of surrounding objects can deteriorate ventilation inside the greenhouse. Gómez-Mataix *et al*. (2012) and Fatnassi *et al*. (2017) studied the spacing

between double-ridge greenhouses at different distances and determined that the best ventilation rates coincide with the largest spacing spans provided by the opening of the double ridge, with the first bay being the best ventilated. The minimum distance between the greenhouse and the obstacle depends on the height of the latter (López *et al*., 2011). Evaluations by He *et al*. (2018) indicate that, in summer, the side window and roof combination provide a better performance for cooling, while in winter, the roof opening is better for dehumidifying the environment.

This study analyzes the effect of a physical barrier on wind trajectory, wind velocity, and temperatures in a passively ventilated gothic-type greenhouse with a tomato crop in the productive stage, installed in a semi-arid environment using numerical simulation techniques.

MATERIALS AND METHODS

Experimental site

The study was carried out in a 14.5 m wide and 80 m long Gothic-type greenhouse covered with translucent polyethylene. The structure has an anti-aphid mesh on the windows, a natural ventilation system, two 3 m high lateral windows, and a 1.4 m zenithal window. It is located at coordinates 23° 59′ 28.87′′ N and 104° 32′ 34.98′′ W, at an altitude of 1868 m. The region has a semi-warm temperate climate with summer rains and an average annual rainfall of around 500 mm, 85 % of which occurs from June to October. The topography is flat, and the soil is alluvial with a loamy texture.

Temperature and relative humidity data were recorded using two Vantage Pro2 Plus stations (Davis Instruments, Hayward, CA, USA), equipped with sensors for ambient temperature (measurement range of 40–65 °C, error ±0.5 °C), relative humidity (measurement range of 1 to 100 %, error ±3 and ±4 % over 90 %), wind velocity (measurement range of 1 to 80 m s^{-1}, error ±5 m s^{-1}), and wind direction (measurement range of 16 compass points, error ±5). The data obtained were stored in the Vantage Pro2 Plus console assigned to each piece of equipment. The stations were placed on the central bed of the crop 40 m from the greenhouse entrance (S3) and outside (in the -z direction, considering the length of the greenhouse), separated 1 m from the air inlet (S6) (Figure 1A).

Four HOBO UX100-003 storage units (Onset Company, Bourne, MA, USA) were also used, with temperature and relative humidity sensors with a measurement range of -40 to 70 °C and 0 to 100 %, and an accuracy of ±0.2 °C and ±2.5 %. Sensors were placed in the central growing bed at 20 and 60 m (S1 and S5, respectively). Sensor S2 was placed 0.5 m from the air inlet and S4 0.5 m from the left window (Figure 1A), both 40 m from the inlet in the -z direction. Data from these sensors were downloaded via Bluetooth using the free HOBOmobile app (Onset Computer Corporation, MA, USA). All variables were measured at canopy height (2 m), including soil temperature (at 0.15 m depth). Data recording was carried out at 10-minute intervals. All windows

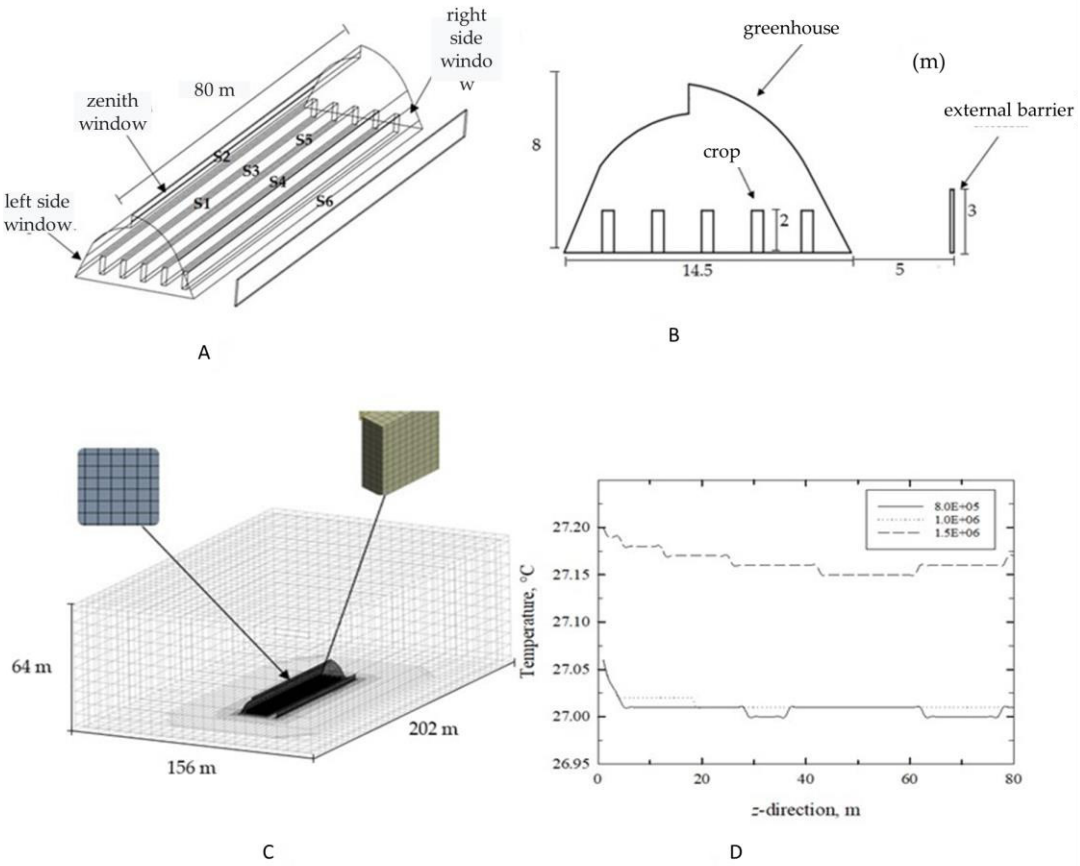

Figure 1. A: geometry isometric view; B: geometry front view; C: meshing, domain dimensions; D: mesh sensitivity analysis.

remained 50 % open during data collection. The study was carried out with an established tomato (*Solanum lycopersicum* L.) crop at the productive stage, 2 m high, distributed in five beds planted in double rows, with mulch.

Development of the computational model

The geometry of the environment is composed of a greenhouse and a barrier placed parallel to the length of the long face of the vessel at a 5 m distance (Figure 1B). The computational domain and total volume dimensions, including the greenhouse, are 156 m wide × 202 m long × 64 m high (Figure 1C). This excess volume guarantees a reliable model according to the recommendations of different authors (Fatnassi *et al*., 2017; Piscia *et al*., 2015). Similarly, a structured type mesh (Figure 1C) consisting of 835 491 elements was considered, with a distortion value of 0.02 and an orthogonal quality of 0.97 on average, indicative of a good fit (Román-Roldán *et al*., 2019; Villagrán

et al., 2020a). The sensitivity analysis of the mesh to calculate the independence of the results on the number of elements (Figure 1D) showed that the numerical model reached a point where the solution does not change significantly by making the mesh more refined, implying that the solution is sufficiently accurate.

Mesh sensitivity analysis was performed by recording 80 temperature points at 2 m from the ground longitudinally in the center of the greenhouse. Three scenarios were analyzed by varying the number of elements in the mesh (He *et al*., 2018; Villagrán *et al*., 2019; Villagrán *et al*., 2020b). The results showed independence in the behavior of temperature in relation to the number of elements; a variation of 0.2 °C is appreciated in the 1 500 000-element mesh compared to the 1 000 000- and 8 000 000-element meshes.

Equations defining fluid dynamics

To solve the fluid dynamic behavior, the Navier-Stokes equations were solved through a matter and energy balance:

$$\frac{\partial \Phi}{\partial t} + \frac{\partial (U\Phi)}{\partial x} + \frac{\partial (V\Phi)}{\partial y} + \frac{\partial (W\Phi)}{\partial z} = -\Gamma \Delta \Phi^2 + S_\Phi$$

where Φ represents the concentration of the dimensionless term, which refers to the amount of motion, mass, or energy; U, V, and W are the components of the velocity vector in three dimensions (m s^{-1}); Γ is the diffusivity coefficient (kg m s^{-1}); and S_Φ is the source term.

The turbulence model used is the two-equation *k-ε*, which has been used in greenhouse simulation (Piscia *et al*., 2015). The Boussinesq hypothesis is considered valid for natural ventilation studies in greenhouses where thermal gradients are below 20 °C. Thus, an inclusion of gravity forces originating from changes in air density due to changes in temperature is performed when solving the momentum equation. The Boussinesq model is represented as follows (Baeza *et al*., 2009; Villagrán *et al*., 2020a):

$$(\rho - \rho_0) g = -\rho_0 \beta (T - T_0) g$$

where β is the coefficient of thermal expansion, g is the force of gravity, and ρ and T are the density and temperature of the air, with the subscript representing a reference state.

Anti-aphid meshes are considered in CFD models as porous jumps due to the pressure drop of the airflowing through them. Bartzanas *et al*. (2004) indicate that meshes can decrease ventilation rates between 33 and 50 % depending on the type, and therefore affect temperature gradients. Darcy's law states that the flow velocity in a porous medium is proportional to the pressure loss due to viscosity effects, but it is violated

in high-velocity flows, which are frequently encountered in the natural environment. To calculate the pressure drop caused by the mesh, the following equation was used (Romero-Gómez *et al*., 2010):

$$\Delta p = -\left(\frac{\mu}{\alpha}v + C_2\frac{1}{2}\rho v^2\right)\Delta J$$

where Δp is the pressure drop (kg m^{-1} s^{-2}), μ is the dynamic flow viscosity (kg m^{-1} s^{-1}), α is the face permeability (m^2), C^2 is the pressure jump coefficient (m^{-1}), and ΔJ is the thickness of the porous jump (m).

Boundary conditions

A symmetry condition was assigned to the front, back, and upper walls of the domain. The air inlet was set at the right wall, according to the predominant wind direction in the region and considering hourly averaged velocity values (Table 1). A pressure outlet was set at the left wall of the domain P = 101.3 kPa (atmospheric pressure). The lower part with soil properties for domain, greenhouse, and cultivation was established as a wall condition. The greenhouse canopy was defined as wall condition v = 0 m s^{-1}. The insect screens on the windows were set as a porous jump, the crop as a porous medium, and the external barrier as a solid wall without slippage, with defined values of the characteristics of the materials considered (Table 2).

Table 1. Hourly averaged climatic variables of the study site for July 5, 2023.

Time	T (°C)	RH (%)	v (m s^{-1})	Time	T (°C)	RH (%)	v (m s^{-1})
06:00	15.13	95	0.2	12:00	27.03	50	0.4
07:00	15.80	96	0.0	13:00	28.95	40	0.0
08:00	17.60	96	0.2	14:00	29.58	34	0.0
09:00	20.35	84	0.0	15:00	31.05	34	0.3
10:00	23.35	69	0.4	16:00	30.20	40	0.6
11:00	25.15	59	0.0	17:00	20.00	79	2.4

Table 2. Physical properties of the materials (Villagrán *et al*., 2020a) used in the mathematical model.

Material	Density (kg m^{-3})	Specific heat (J kg^{-1} K^{-1})	Thermal conductivity (W m^{-1} K^{-1})
Plastic	925.5	1600	0.33
Crop	1000	4180	0.6
Soil	1400	1738	1.5
Air	1.225	1006.46	0.0242
Brick	1700	800	1.31

Case studies

The greenhouse is built on a plot of land with a perimeter fence on the right side, 5 m away. This configuration was used to validate the numerical simulation. Once validated, four scenarios were analyzed, feeding the same environmental conditions at three different times of the day (6:00, 14:00, and 17:00 h) to study the variations in thermal and wind behavior.

To generate a solution, a pressure-based algorithm was used, where a convergence value of 1×10^{-6} was established and the following considerations, demonstrated by various authors, were taken into account (Flores-Velázquez *et al*., 2014; Piscia *et al*., 2015; Aguilar-Rodríguez *et al*., 2020b; Si *et al*., 2023): a) the energy equation is solved, b) the temperature and wind velocity profiles are constant, c) there is a pressure jump in the windows caused by the antiaphid meshes (Table 3), d) the crop behaves as a porous medium, and e) the air density is affected by the Boussinesq effect.

For each scenario, a 50 % window opening was considered as this was the greenhouse's operating conditions at the time of data collection. The crop (tomato) in production stage was considered as a barrier. Crop transpiration was not considered in the simulation, since the trajectory of wind currents and their influence on the thermal field was evaluated. The case studies and an illustration of the computational domain are shown (Table 4). The numerical models were solved using the commercial software Ansys Fluent®.

Table 3. Physical characteristics of the antiaphid netting used in the mathematical model.

Property	Measure
Face permeability	2.86×10^{-9} m^2
Thickness of porous medium	3.72×10^{-4} m
Pressure drop coefficient	11 131.45 m^{-1}
Thermal resistance	0

Table 4. Study cases varying the barrier position. A: no barrier; B: barrier at 5 m; C: barrier at 10 m; D: barrier at 15 m.

Case	Barrier position	Geometry
A	No barrier	
B	5 m (validation)	
C	10 m	
D	15 m	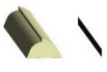

RESULTS AND DISCUSSION

Model validation

The data used were those obtained by the sensors on July 5, 2023. The model was evaluated during the diurnal period between 6:00 and 18:00 h, recording the climatic conditions of the study site on an hourly average (Table 1). Mean absolute error (MAE), root mean square error (RSME), and R^2 were calculated as measures of data goodness-of-fit, as they adequately allow determining the reliability of the model:

$$MAE = \frac{1}{n}\sum_{i=1}^{n}|real_i - simulated_i|$$

$$RSME = \sqrt{\frac{\sum_{i=1}^{n}|real_i - simulated_i|^2}{n}}$$

$$R^2 = 1 - \frac{\sum_{i=1}^{n}|real_i - simulated_i|^2}{\sum_{i=1}^{n}\left|real_i - \overline{real}\right|^2}$$

Values of MAE = 1.5, RSME = 2.5, and R^2 = 0.869 were obtained, indicating that the model has a good fit with the experimental data (Villagrán *et al*., 2019; Román-Roldán *et al*., 2019; Villagrán *et al*., 2020b). The average error was ±1.5 °C, suggesting that the simulated values are not far away from the real values. A higher RMSE value compared to MAE indicates that the model presents a lower predictive capacity at some points. This is demonstrated by the correlation between the computed and measured data at various times of the day (Figure 2). In addition, the regression curve is shown, where it can be observed that the dispersion is 14 %.

Velocity fields

This analysis was performed indirectly in the absence of wind sensors inside the greenhouse, but based on temperature measurements, as reported by Villagrán and Bojacá (2019). The observed behaviors for wind velocities lower than 1 m s^{-1} presented similar behavior among themselves, so the analysis was performed on the simulated case with v = 2.4 m s^{-1} and T = 20 °C outside the greenhouse in the transverse profile obtained at 40 m (-z axis), where the most notorious temperature and velocity gradients are concentrated. The vectors described a behavior that agrees with the wind trajectory diagrams reported by Kacira *et al*. (2004) and Baeza *et al*. (2009).

The comparison between the four case studies shows that, in the absence of the barrier, vectors with constant velocity and trajectory are observed until they reach the greenhouse window, where the velocity is reduced by the presence of the insect

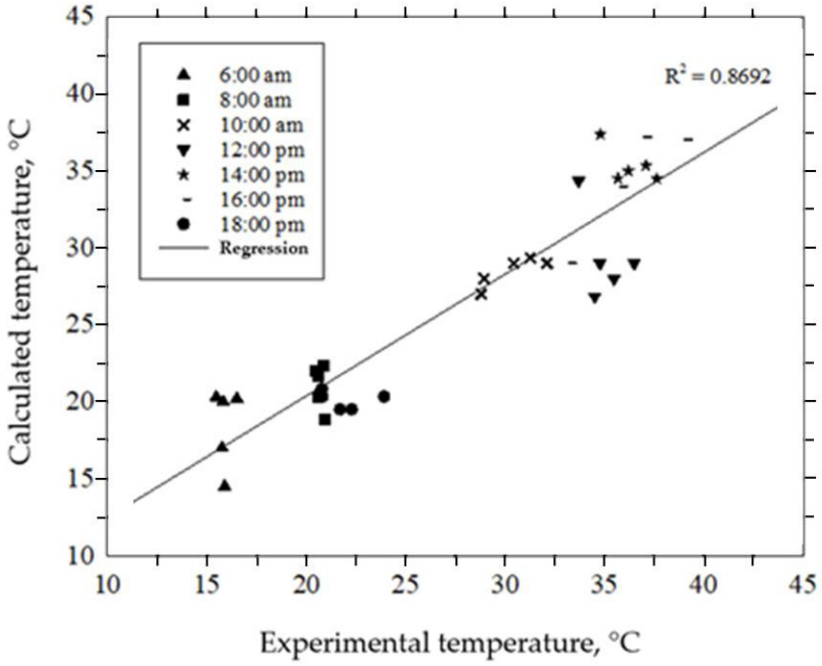

Figure 2. Validation of the computational model, recording hourly averaged measurements from each sensor.

screen (Figure 3A, point 1). Inside the greenhouse, the airflow rises and crosses the greenhouse, exiting through the left and zenith windows; this flow creates a recirculation at point 2 as it comes into contact with the air moving through the crop driven by the temperature difference.

With the presence of the external barrier at 5, 10, and 15 m, at points 3, 6, and 7 (Figure 3B-D), the recirculation formed between the greenhouse and the barrier decreases the airflow at the entrance. Regardless of the position of the external barrier, the airflow inside the greenhouse at the entrance of the right window is between 0 and 0.5 m s^{-1}, in contrast to the case without the barrier, where the velocity is up to 1.2 m s^{-1}. Although the velocity with which the air reaches the right greenhouse window decreases with increasing distance between the vessel and the barrier (1.6, 1, and 0.85 m s^{-1} for 5, 10, and 15 m, respectively), no changes in the velocity inside the vessel are observed.

By reducing the air entry in the right window, airflow through the left and zenith windows is promoted, and the formation of recirculation within the greenhouse at points 4, 6, and 8 is favored (Figure 3B–D). This affects the trajectory of the vectors through the crop and forces the flow of hot air to remain in these areas. The velocity of 0–0.2 m s^{-1} inside the shed in all cases with the external barrier indicates that the air current movement is due to the temperature difference (Kacira *et al*., 2004). In cases with data obtained at 2 and 4 m height and 40 m in the -*z* direction (Figure 4), the best

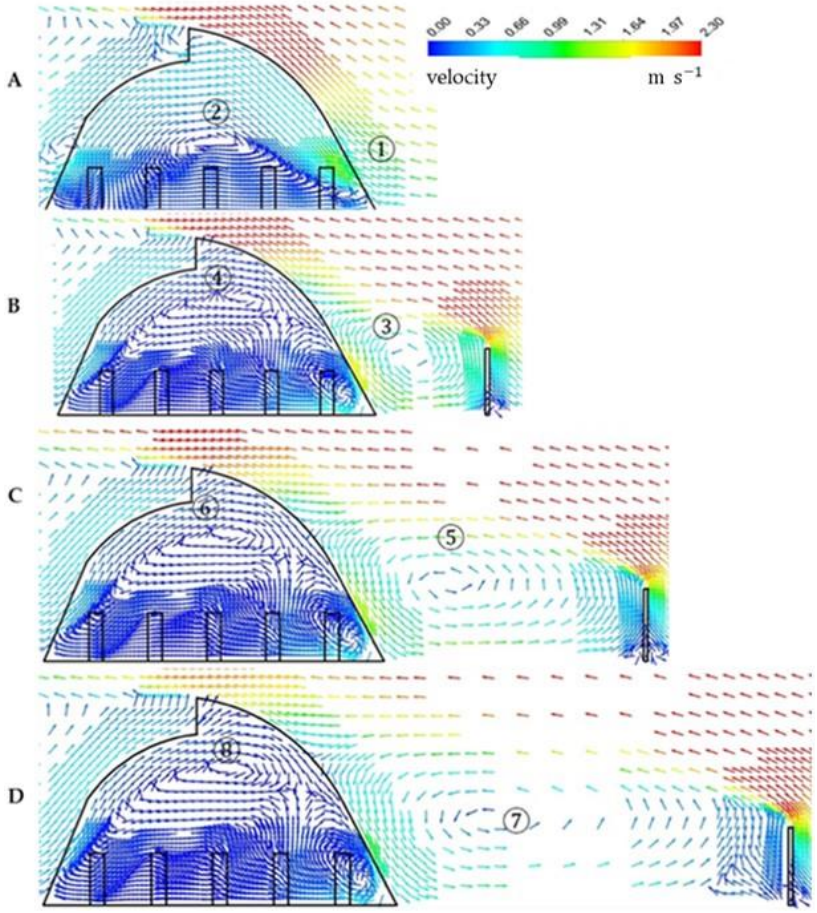

Figure 3. Wind velocity and trajectory profile projected at 18:00 h. A: no barrier; B: barrier at 5 m; C: barrier at 10 m; D: barrier at 15 m.

ventilation conditions correspond to the scenario without the presence of the external barrier, which agrees with Fatnassi *et al*. (2017). It is also observed that it does not cause a total obstruction in ventilation due to the height of the barrier (3 m) (López *et al*., 2011).

On the other hand, all scenarios with barriers had lower values of velocity at crop height (0.1–0.2 m s^{-1}) (Figure 4). The simulation results showed higher wind velocity at 4 m from the ground, where the recirculation formed by the flows between the left and zenith windows was generated. This promoted velocities at the center of the greenhouse of 0.3–0.2 m s^{-1} for the cases with the barrier at 5 and 15 m, respectively. The barrier at 10 m maintained uniform velocity values of less than 0.1 m s^{-1}. The recirculation does not affect the crop level, but it does influence the movement of the airflow through it (Akrami *et al*., 2020).

The highest velocity was reached in the case without a barrier (1.4 m s^{-1} at the entrance, which decreased to 0.35 m s^{-1} in the center of the greenhouse to increase again at the

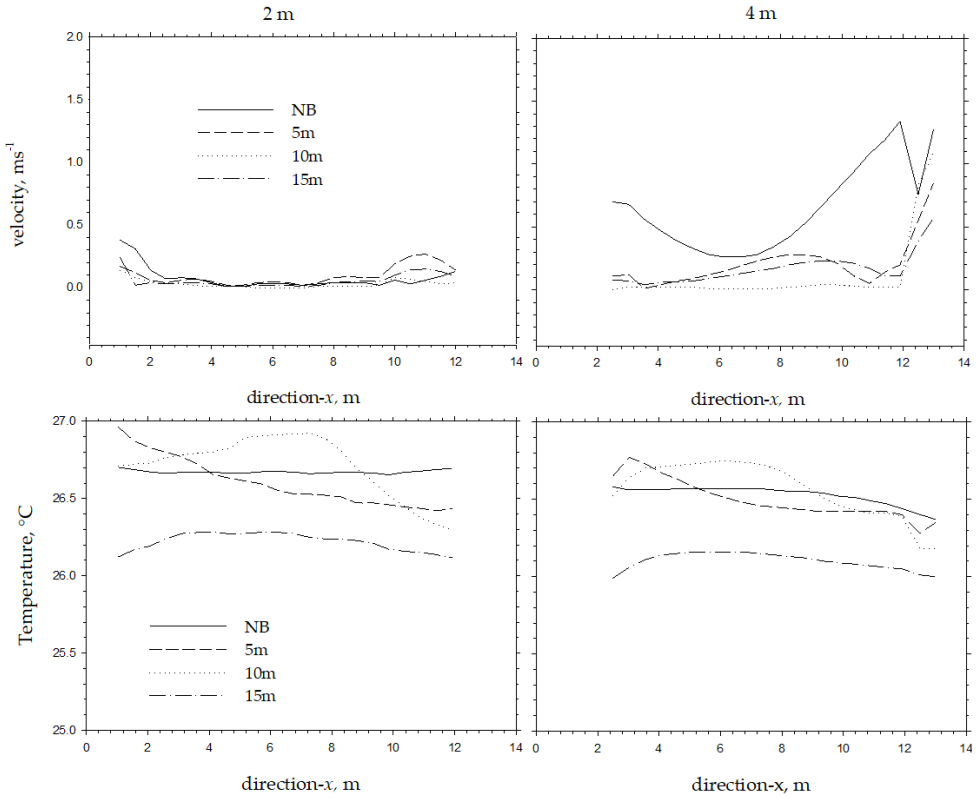

Figure 4. Wind and temperature behavior at 2 and 4 m height for the cases without barrier, with barrier at 5 m, barrier at 10 m, and barrier at 15 m in the -*x* and -*z* directions.

exit through the left window), where no recirculation was formed at that height, but a flow from the right window to the left and zenith window was observed. On the other hand, for the wind velocity that was simulated, the changes in temperature were not caused by the airflow but by convective phenomena. The scenario that presented the lowest temperature was the barrier at 10 m (Figure 4), with variations of about 1 °C when compared to the other scenarios, which indicates that with the simulated conditions at 18:00 h, the presence or placement of the barrier does not represent a significant temperature change for the crop.

Temperature contours

To analyze the thermal behavior inside the greenhouse, three planes were analyzed in the transverse profile, located at 20, 40, and 60 m (-*z*-axis) and a plane 2 m above the ground, which corresponds to the height of the canopy. The thermal distribution at 6:00 and 14:00 h was analyzed to identify the times of lowest and highest temperature in the study region for a common day in July (Figure 5). At 6:00 h, with an external temperature of 15.13 °C and wind velocity of 0.2 m s^{-1}, the temperature profile is the

most homogeneous in the no-barrier scenario (Figure 5, A–A'), where a temperature of ~19 °C predominates at the center of the greenhouse at crop height due to the heat emanating from the ground and its distance from the windows, where the temperature is ~18 °C.

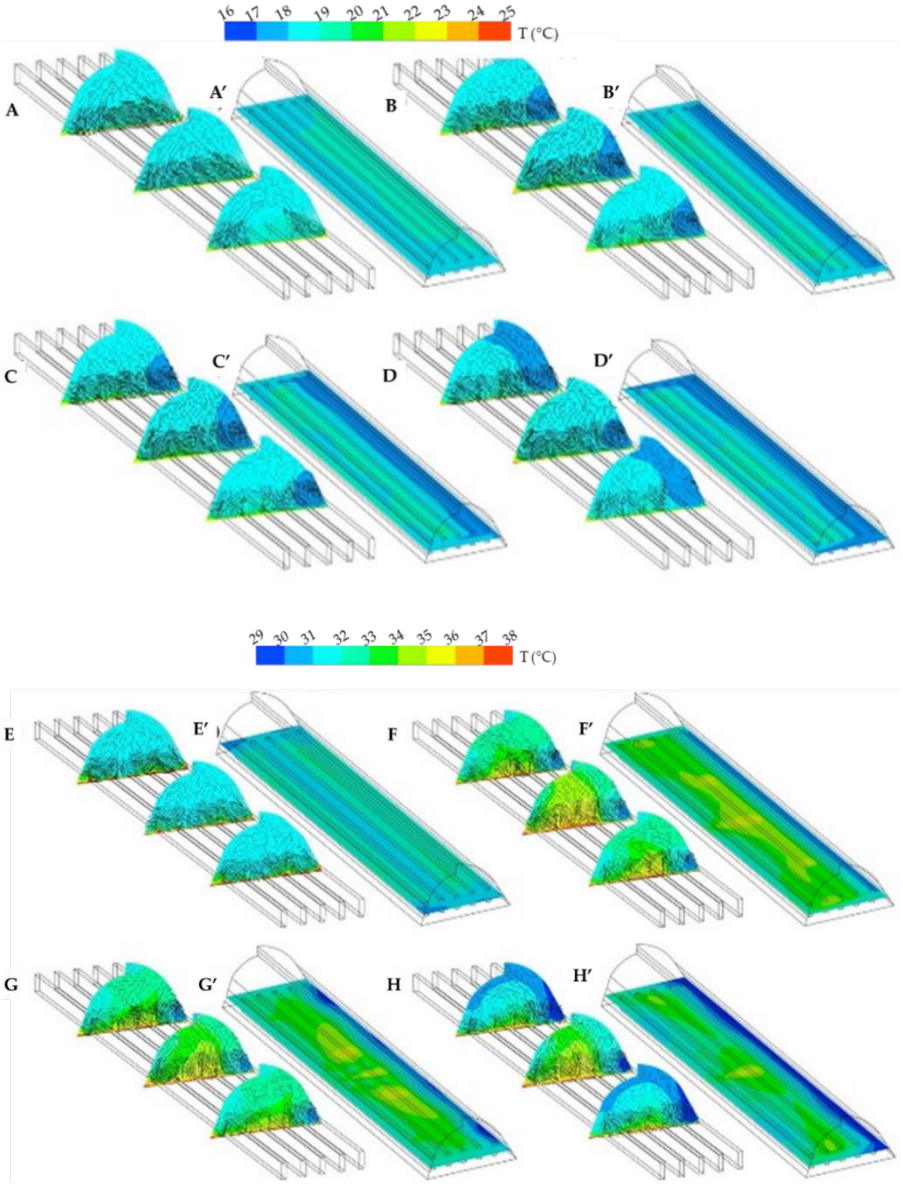

Figure 5. Greenhouse temperature profiles at 6:00 am: A: no barrier; B: barrier at 5 m; C: barrier at 10 m; D: barrier at 15 m. Temperature profiles at 14:00 h: E: no barrier; F: barrier at 5 m; G: barrier at 10 m; H: barrier at 15 m. A'–H': thermal contours in the transverse planes for the case without barrier and at 5, 10, and 15 m, at 6:00 and 14:00 h, respectively.

In the cases with a barrier at 5 and 10 m, a deflection is observed in the inflow current that forms a vortex next to the right window and maintains the temperature at ∼17 °C in this area (Figure 5, B–B′ and C–C′), which caused an increase of up to 4 °C compared to the case without a barrier, obtaining temperatures of 23 °C at the center of the vessel and decreasing to 21 °C at the left window for the case with a barrier at 5 m.

For the case with the barrier at 10 m, the temperature was 20 °C in the left window and 22 °C in the center; this is due to the limitation that the barrier offers to the entry of cold air, which allows temperatures of 20–23 °C to cover approximately 85 % of the building at canopy height. Since this increase in temperature is proportional to the proximity of the barrier, in the case where the barrier is located at 15 m (Figure 5, D–D′), the low temperature containment next to the window mentioned in the cases at 5 and 10 m was not generated. For this case (at 15 m), the lower temperature (18 °C) was not only located at the entrance of the right window but extended to the upper part of the greenhouse, adjacent to the right wall of the greenhouse and up to the zenith window.

Also, a lower temperature was observed at the front and rear ends of the greenhouse, so that the values of 22 °C were concentrated from the middle zone of the greenhouse towards the left window, where a decrease of 1 °C was observed. Despite a very low wind velocity (0.2 m s^{-1}), the change in internal temperature with the presence of the barrier was observed. According to the simulation, the optimum temperatures were obtained when the barrier was 5 m away, showing a homogeneous behavior and a greater positive temperature gradient with respect to the outside temperature (5–6 °C).

In the profiles corresponding to 14:00 h, where the external temperature is ∼29 °C and the wind velocity is ∼1.8 m s^{-1} with no barrier (Figure 5, E–E′), a uniform temperature profile was shown due to the behavior of the air currents (Figure 3A). In this case, wind velocities barely reach 0.2 m s^{-1} in most of the greenhouse, so it is not a determining factor in the temperature change, which remains at 31 °C, but the direction of the currents formed by the difference in densities is. In the cases with barriers at 5 and 10 m (Figure 5, F–F′ and G–G′), their presence caused lower temperatures at the air inlet (30 °C), the center, and the left window (31–32 °C), keeping the temperature distribution uniform in all cases in the -*z* direction. At canopy height, a variation of only 0.5 °C was observed between the exposed scenarios.

Contrary to the plans described above, in the case of the presence of the barrier at 15 m (Figure 5, H–H′), there was a more noticeable temperature decrease towards the top on the right wall, which caused a difference of 1 °C compared to the center of the greenhouse. However, it only reached the first row of crops, while in the rest of the greenhouse a homogeneous temperature of 30–31 °C was obtained.

The four study cases were analyzed by plotting the temperature of each of them at a height of 2 m in the central part of the greenhouse in the -x and -z directions. At 6:00 h, the case without a barrier showed the lowest temperature (Figure 6), which remained uniform in the -*z* direction (18.5 °C) and showed a variation of approximately 1 °C

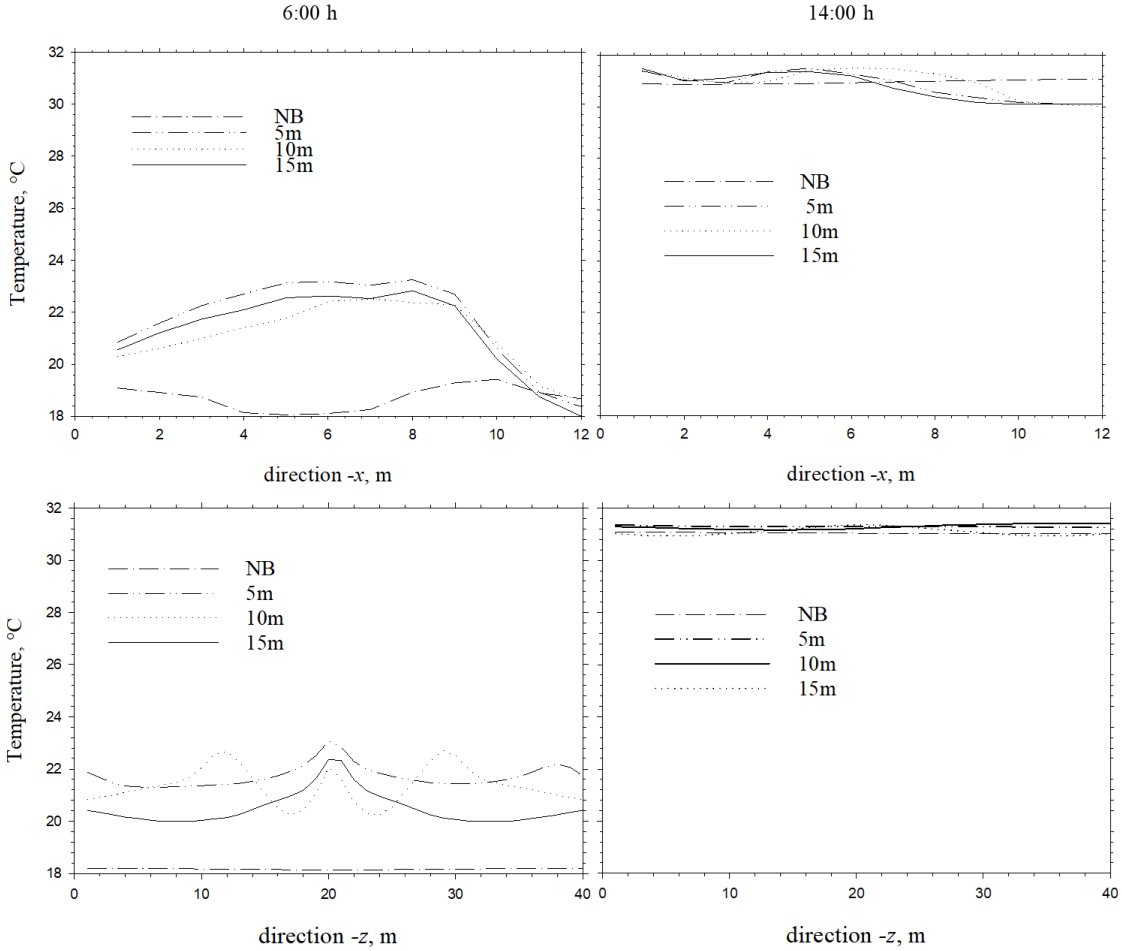

Figure 6. Temperature behavior at 6:00 and 14:00 hours on July 5, 2023, for the cases without a barrier, barrier at 5 m, barrier at 10 m, and barrier at 15 m in the *-x* and *-z* directions.

along the -x direction. The case with a barrier at 5 m showed the highest temperature on the *-x* axis (23 °C) compared to the cases with a barrier at 10 and 15 m; this temperature was reached at the center of the vessel, decreasing to 22 °C as the line approaches the right and left ends of the greenhouse.

These 22 °C coincide along the *-z* axis, indicating that the presence of the barrier placed at 5 m allows maintaining the temperature 4 to 5 °C higher during the coldest hours than in the case without a barrier. This phenomenon was not observed at 14:00 h, where the presence of the barrier did not show changes in the thermal behavior of the greenhouse, with differences of only 0.5 °C in the *-z* direction and 1 °C in the *-x* direction, where the average temperature for the four cases remained at 31 °C.

CONCLUSIONS

The presence of the external physical barrier, regardless of its distance, decreased ventilation inside the greenhouse by up to 60 %, modifying the trajectory of the air current outside and inside the greenhouse. Inside, the flow path was affected in the same way, regardless of the distance from the barrier; however, the temperature at canopy height increased between 2 and 4 °C depending on its placement. The barrier located at 5 m was useful in the summer climate to slow the temperature drop at dawn, maintaining up to 4 °C above the external temperature. The most homogeneous ventilation and temperature distribution were obtained in the absence of the barrier. It is suggested that the results of this study be taken into account in the design of greenhouses located in urban areas.

ACKNOWLEDGEMENTS

The authors wish to thank the TecNM-ITM, SNI, TecNM-ITVG for the scholarship granted for the DCI graduate studies, FIM-UMSNH, and Dr. José de Jesús Muñoz Ramos, research professor of the TecNM-ITVG, for the support provided to carry out this study.

REFERENCES

Aguilar-Rodríguez CE, Flores-Velázquez J, Ojeda-Bustamante W, Rojano F, Iñiguez-Covarrubias M. 2020a. Valuation of the energy performance of a greenhouse with an electric heater using numerical simulations. Processes 8 (5): 600. https://doi.org/10.3390/pr8050600

Aguilar-Rodríguez CE, Flores-Velázquez J, Rojano F, Flores-Magdaleno H, Rubiños-Panta E. 2021. Simulation of water vapor and near infrared radiation to predict vapor pressure deficit in a greenhouse using CFD. Processes 9 (9): 1587. https://doi.org/10.3390/pr9091587

Aguilar-Rodríguez CE, Flores-Velázquez J, Rojano-Aguilar F, Ojeda-Bustamante W, Iñiguez-Covarrubias M. 2020b. Tomato (*Solanum lycopersicum* L.) crop cycle estimation in greenhouse, based on degree day heat (GDC) simulated in CFD. Tecnología y Ciencias del Agua 11 (4): 27–59. https://doi.org/10.24850/j-tyca-2020-04-02

Akrami M, Javadi AA, Hassanein MJ, Farmani R, Dibaj M, Tabor GR, Negm A. 2020. Study of the effects of vent configuration on mono-span greenhouse ventilation using computational fluid dynamics. Sustainability 12 (3): 986. https://doi.org/10.3390/su12030986

Baeza EJ, Pérez-Parra JJ, Montero JI, Bailey BJ, López JC, Gázquez JC. 2009. Analysis of the role of sidewall vents on buoyancy-driven natural ventilation in parral-type greenhouses with and without insect screens using computational fluid dynamics. Biosystems Engineering 104 (1): 86–96. https://doi.org/10.1016/j.biosystemseng.2009.04.008

Bartzanas T, Boulard T, Kittas C. 2004. Effect of vent arrangement on windward ventilation of a tunnel greenhouse. Biosystems Engineering 88 (4): 479–490. https://doi.org/10.1016/j.biosystemseng.2003.10.006

Bournet PE, Rojano F. 2022. Advances of computational fluid dynamics (CFD) applications in agricultural building modelling: Research, applications and challenges. Computers and Electronics in Agriculture 201: 107277. https://doi.org/10.1016/j.compag.2022.107277

Carpentieri M, Robins AG. 2015. Influence of urban morphology on airflow over building arrays. Journal of Wind Engineering and Industrial Aerodynamics 145: 61–74. https://doi.org/10.1016/j.jweia.2015.06.001

Castro IP, Xie ZT, Fuka V, Robins AG, Carpentieri M, Hayden P, Hertwig D, Coceal O. 2017. Measurements and computations of flow in an urban street system. Boundary-Layer Meteorology 162 (2): 207–230. https://doi.org/10.1007/s10546-016-0200-7

Choab N, Allouhi A, El-Maakoul A, Kousksou T, Saadeddine S, Jamil A. 2019. Review on greenhouse microclimate and application: Design parameters, thermal modeling and simulation, climate controlling technologies. Solar Energy 191: 109–137. https://doi.org/10.1016/j.solener.2019.08.042

Chu CR, Lan TW. 2019. Effectiveness of ridge vent to wind-driven natural ventilation in monoslope multi-span greenhouses. Biosystems Engineering 186: 279–292. https://doi.org/10.1016/j.biosystemseng.2019.08.006

El-Alaoui M, Chahidi L, Rougui M, Mechaqrane A, Allal S. 2023. Evaluation of CFD and machine learning methods on predicting greenhouse microclimate parameters with the assessment of seasonality impact on machine learning performance. Scientific African 19: e01578. https://doi.org/10.1016/j.sciaf.2023.e01578

Espinoza K, López A, Valera DL, Molina-Aiz FD, Torres JA, Peña A. 2017. Effects of ventilator configuration on the flow pattern of a naturally-ventilated three-span Mediterranean greenhouse. Biosystems Engineering 164: 13–30. https://doi.org/10.1016/j.biosystemseng.2017.10.001

Fatnassi H, Boulard T, Benamara H, Roy JC, Suay R, Poncet C. 2017. Increasing the height and multiplying the number of spans of greenhouse: How far can we go? Acta Horticulturae 1170: 137–144. https://doi.org/10.17660/ActaHortic.2017.1170.15

Flores-Velázquez J, López-Cruz IL, Mejía-Sáenz E, Montero-Camacho JI. 2014. Evaluación del desempeño climático de un invernadero baticenital del centro de México mediante dinámica de fluidos computacional (CFD). Agrociencia 48 (2): 131–146.

Flores-Velázquez J, Ojeda-Bustamante W. 2015. Consideraciones agronómicas para el diseño de invernaderos típicos de México. Secretaría de Medio Ambiente y Recursos Naturales. Jiutepec, México. 179 p.

Ghoulem M, Moueddeb K, Nehdi E, Zhong F, Calautit J. 2020. Analysis of passive downdraught evaporative cooling windcatcher for greenhouses in hot climatic conditions: Parametric study and impact of neighboring structures. Biosystems Engineering 197: 105–121. https://doi.org/10.1016/j.biosystemseng.2020.06.016

Gómez-Mataix G, Montero JI, Raya V, Suay R. 2012. Benchmark study of the distance between greenhouses and its effect on wind driven ventilation. Acta Horticulturae 1008: 207–211 https://doi.org/10.17660/ActaHortic.2013.1008.27

He X, Wang J, Guo S, Zhang J, Wei B, Sun J, Shu S. 2018. Ventilation optimization of solar greenhouse with removable back walls based on CFD. Computers and Electronics in Agriculture 149: 16–25. https://doi.org/10.1016/j.compag.2017.10.001

Kacira M, Sase S, Okushima L. 2004. Effects on side vents and span numbers on wind-induced natural ventilation of a Gothic multi-span greenhouse. Japan Agricultural Research Quarterly 38 (4): 227–233. https://doi.org/10.6090/jarq.38.227

King MF, Gough HL, Halios C, Barlow JF, Robertson A, Hoxey R, Noakes CJ. 2017. Investigation of the influence of neighboring structures on the natural ventilation potential of a full-scale cubic building using time-dependent CFD. Journal of Wind Engineering and Industrial Aerodynamics 16: 265–279. https://doi.org/10.1016/j.jweia.2017.07.020

Li H, Li Y, Yue X, Liu X, Tian S, Li T. 2020. Evaluation of airflow pattern and thermal behavior of the arched greenhouses with designed roof ventilation scenarios using CFD simulation. PloS One 15 (9): e0239851. https://doi.org/10.1371/journal.pone.0239851

López A, Valera DL, Molina-Aiz FD, Peña A. 2011. Effects of surrounding buildings on air patterns and turbulence in two naturally ventilated Mediterranean greenhouses using tri-sonic anemometry. Transactions of the ASABE 54 (5): 1941–1950. https://doi.org/10.13031/2013.39835

Ortiz-Rocha GA, Pichimata MA, Villagrán E. 2021. Research on the microclimate of protected agriculture structures using numerical simulation tools: A technical and bibliometric analysis as a contribution to the sustainability of under-cover cropping in tropical and subtropical countries. Sustainability 13 (18): 10433. https://doi.org/10.3390/su131810433

Piscia D, Muñoz P, Panadés C, Montero JI. 2015. A method of coupling CFD and energy balance simulations to study humidity control in unheated greenhouses. Computers and Electronics in Agriculture 115: 129–141. https://doi.org/10.1016/j.compag.2015.05.005

Román-Roldán NI, López-Ortiz A, Ituna-Yudonago JF, García-Valladares O, Pilatowsky-Figueroa I. 2019. Computational fluid dynamics analysis of heat transfer in a greenhouse solar dryer "chapel-type" coupled to an air solar heating system. Energy Science and Engineering 7 (4): 1123–1139. https://doi.org/10.1002/ese3.333

Romero-Gómez P, Choi CY, Lopez-Cruz IL. 2010. Enhancement of the greenhouse air ventilation rate under climate conditions of central Mexico. Agrociencia 44 (1): 1–15.

Ruiz-García A, López-Cruz I, Arteaga-Ramírez R, Ramírez-Arias JA. 2015. Natural ventilation rates of a greenhouse at central Mexico estimated by energy balance. Agrociencia 49 (1): 87–100.

Si C, Qi F, Ding X, He F, Gao Z, Feng Q, Zheng L. 2023. CFD Analysis of solar greenhouse thermal and humidity environment considering soil-crop-back wall interactions. Energies 16 (5): 2305. https://doi.org/10.3390/en16052305

Villagrán E, León R, Rodríguez A, Jaramillo J. 2020a. 3D Numerical analysis of the natural ventilation behavior in a Colombian greenhouse established in warm climate conditions. Sustainability 12 (19): 8101. https://doi.org/10.3390/su12198101

Villagrán EA, Baeza-Romero EJ, Bojacá CR. 2019. Transient CFD analysis of the natural ventilation of three types of greenhouses used for agricultural production in a tropical mountain climate. Biosystems Engineering 188: 288–304. https://doi.org/10.1016/j.biosystemseng.2019.10.026

Villagrán EA, Bojacá CR. 2019. Effects of surrounding objects on the thermal performance of passively ventilated greenhouses. Journal of Agricultural Engineering 50 (1): 20–27. https://doi.org/10.4081/jae.2019.856

Villagrán EA, Jaramillo JE, León-Pacheco RI. 2020b. Ventilación natural en invernadero con mallas anti-insecto evaluadas con un modelo computacional de fluidos. Agronomía Mesoamericana 31 (3): 698–717. https://doi.org/10.15517/am.v31i3.40782